ORNL-3893
UC-34 – Physics

ABSOLUTE EFFICIENCY MEASUREMENTS OF NE-213 ORGANIC PHOSPHORS FOR DETECTING 14.4- AND 2.6-MeV NEUTRONS

T. A. Love
R. T. Santoro
R. W. Peelle
N. W. Hill

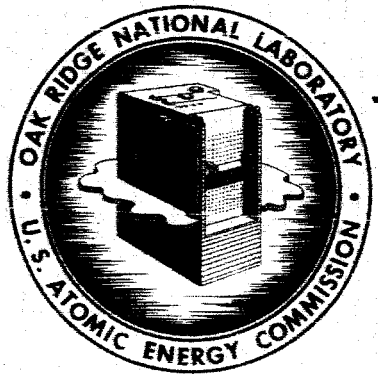

OAK RIDGE NATIONAL LABORATORY
operated by
UNION CARBIDE CORPORATION
for the
U.S. ATOMIC ENERGY COMMISSION

Printed in USA. Price $3.00 . Available from the Clearinghouse for Federal Scientific and Technical Information, National Bureau of Standards, U.S. Department of Commerce, Springfield, Virginia 22151

ORNL-3893

Contract No. W-7405-eng-26

Neutron Physics Division

ABSOLUTE EFFICIENCY MEASUREMENTS OF NE-213 ORGANIC PHOSPHORS FOR DETECTING 14.4- AND 2.6-MeV NEUTRONS

T. A. Love, R. T. Santoro, R. W. Peelle, and N. W. Hill*

NOTE:

This Work Partially Supported by
NATIONAL AERONAUTICS AND SPACE ADMINISTRATION
Under Order R-104(1)

SEPTEMBER 1966

*Instrumentation and Controls Division.

OAK RIDGE NATIONAL LABORATORY
Oak Ridge, Tennessee
operated by
UNION CARBIDE NUCLEAR COMPANY
for the
U.S. ATOMIC ENERGY COMMISSION

TABLE OF CONTENTS

ABSTRACT

The absolute efficiency of two NE-213 organic scintillators for detecting 2.6- and 14.4-MeV neutrons has been determined by the associated particle technique with the recoil particles from the $D(d,n)^3He$ and $T(d,n)^4He$ reactions. The scintillators are 12 cm in diameter and have thicknesses of 2.61 and 6.10 cm. This report describes the efficiency measurements, the detector arrangement, and the function of the associated electronic circuitry, including the pulse-crossover-time pulse-shape discrimination system and the fast circuits used to time helium recoils in a thin silicon detector. The output of the neutron detector was placed in coincidence with the helium recoil pulses, and the efficiency of the detector was obtained as the ratio of the coincidence counts to the helium recoil counts. Measurements were made as a function of the bias level of a tunnel diode driven by the current pulse from dynode 14 of a 58AVP multiplier phototube and also as a function of a bias threshold on the total light output. The bias level was calibrated in terms of pulse-height spectra resulting from interactions in the phosphors of gamma rays of various energies. The results given are for a detector system which included a 5-mm NE-102 slab in front of the NE-213 scintillator and a 3.3-cm (average thickness) Lucite light pipe. Results are given for specified fast-light thresholds and for total light thresholds above about 160-keV electron-equivalent. Comparisons are made between experimental results and results obtained by Monte Carlo analysis. For a threshold of 400 ± 5 keV electron total light equivalent, typical measured detection efficiencies for the smaller detector are 0.122 ± 0.001 and 0.092 ± 0.001 for 2.66- and 14.4-MeV neutrons, respectively. Corresponding calculated values are 0.114 ± 0.001 and 0.095 ± 0.001. For the larger detector the measured efficiencies are 0.245 ± 0.001 and 0.203 ± 0.001 for 2.66- and 14.4-MeV neutrons, respectively, and the calculated values are 0.247 ± 0.003 and 0.200 ± 0.002.

I. INTRODUCTION

The use of NE-213 liquid scintillators* as the sensitive element in neutron detectors, including spectrometers, has become fairly widespread in recent years.[1-6] Some of the advantages of these organic phosphors are that they are available in a wide variety of sizes and shapes, they have a high sensitivity to neutrons, and they have a variation in decay time which through pulse-shape discrimination permits pulses due to electrons to be separated from those due to protons and alpha particles. The absolute efficiencies of two such scintillators for detecting 2.6- and 14.4-MeV neutrons, at various threshold settings, have been determined in a series of experiments in which the associated particle technique[7,8] was used on the recoil particles from the $D(d,n)^3He$ and $T(d,n)^4He$ reactions. The scintillators are 12 cm in diameter and have thicknesses of 2.61 and 6.10 cm. In some cases the measured efficiencies are compared with values computed by the Monte Carlo method.

II. THEORY OF THE ASSOCIATED-PARTICLE TECHNIQUE

In the center-of-mass system for the $D(d,n)^3He$ and $T(d,n)^4He$ reactions, each neutron has associated with it a helium ion emitted at an angle of 180° with respect to the emitted neutron. Determination of the energy of the helium particle and its direction with respect to the incident deuteron determines, from the kinematics of the reaction, the energy and angle of emission of the corresponding neutron. If the helium particles are

*NE-213 is a liquid scintillator manufactured by Nuclear Enterprises, Ltd., Winnepeg, Canada. Its hydrogen and carbon densities are 5.51 and 4.55×10^{22} atoms/g, respectively; sp gr = 0.8752 at 23°C; pulse height = 78% anthracene; decay constant = 2×10^{-9} sec; wavelength of maximum emission = 4300 Å.

detected within a well-defined solid angle and counted, the number, angle, and time relations of the conjugate neutrons are known. If a hydrogenous scintillator is so placed that all the neutrons conjugate to the counted alpha particles pass through a uniform thickness of the scintillator, and if pulses arising from interactions of these neutrons in the scintillator are counted above a given threshold in coincidence with the associated alpha particles, the efficiency of the neutron detector above the given pulse-height threshold may be obtained from the ratio

$$\epsilon = \frac{\text{coincidence counts}}{\text{charged particle counts}}$$

provided proper precautions are taken.

One of the precautions consists in identifying the reaction products of competing reactions and rejecting those not associated with the reaction which produces the neutrons under measurement. At the incident energies used for this experiment, the only competing reaction that is important is the $D(d,p)^3H$ reaction, but it must be considered both during the measurements employing the $D(d,n)^3He$ reaction and during the experiments using the $T(d,n)^4He$ reaction, the latter because the tritium target gradually becomes contaminated with deuterium from the incident beam. The $D(d,n)^3He$ and $D(d,p)^3H$ reactions are about equally probable, and the resulting ^3He and ^3H particles have very nearly the same energy. The ^4He particle from the $T(d,n)^4He$ reaction also has approximately the same energy as the proton from the D + D reaction.

The several factors influencing the monochromaticity of the neutrons must also be considered: the $\pm 5.2^{\circ}$ angular spread through which the

charged particles are accepted, the ±5-keV spread in deuteron beam energy the degradation of the incident deuteron beam in energy as it traverses the "thick" targets used, and the wide angle scattering of the incident deuterons. For the experiments described in this report the neutron energy spread due to the wide-angle scattering of the incident deuteron dominates, as may be seen from Table 1; however, of the wide-angle-scattered deuterons, only about 2% are scattered at an angle of 30° or greater, and 20% are scattered at an angle of $>10^{\circ}$.

The effect on the average energy of the neutrons due to acceleration of D_2^+ or HD^+ instead of D^+ is believed to be small.

III. DESCRIPTION OF THE APPARATUS

A block diagram of the components used in this experiment is shown in Fig. 1. The deuteron beam was obtained from a particle accelerator driven by a Sames electrostatic generator. Mounted at the end of the beam tube was a target and charged-particle-detector assembly which served to orient the target in the incident beam and position the detector with respect to the target.

Targets

Both the deuterium and the tritium targets were obtained from the ORNL Isotopes Division. The tritium targets were made by saturating 500-$\mu g/cm^2$-thick titanium layers with tritium. The layers had been evaporated on 20-mil silver backing plates. The tritium activity varied from 1 to 1.5 curies on a $\frac{1}{2}$-in.-diam active region.

Table 1. Energy Spread of Fast Neutrons Induced by Tested Experimental Conditions

Factor Influencing Neutron Energy Spread	Neutron Energy Spread (keV)	
	$D(d,n)^3He$ Reaction[a] [E_d = 85 ± 5 keV; E_m (avg.) = 2.66 MeV]	$T(d,n)^4He$ Reaction[a] [E_d = 135 ± 5 keV; E_m (avg.) = 14.43 MeV]
±5 keV in beam energy	±10	±30
±5.20 in acceptance angle of charged particle determined	±38	±75
Target thickness[b]	+50 -100	+300 -200
Wide-angle scattering of incident deuteron	±250	±600
Combined spread	±265	±650

a. The reaction charged particles observed were those emitted at 120 ± 5 deg.

b. The slowing down of the deuterons in a thick target allowed the deuteron to react with all E_d from E_d = max to E_d = 0. This condition also produced an angular spread of neutrons for the fixed 120 deg helium ion direction: ±7 deg for the D(d,n) reaction and ±2.0 deg for the T(d,n) reaction.

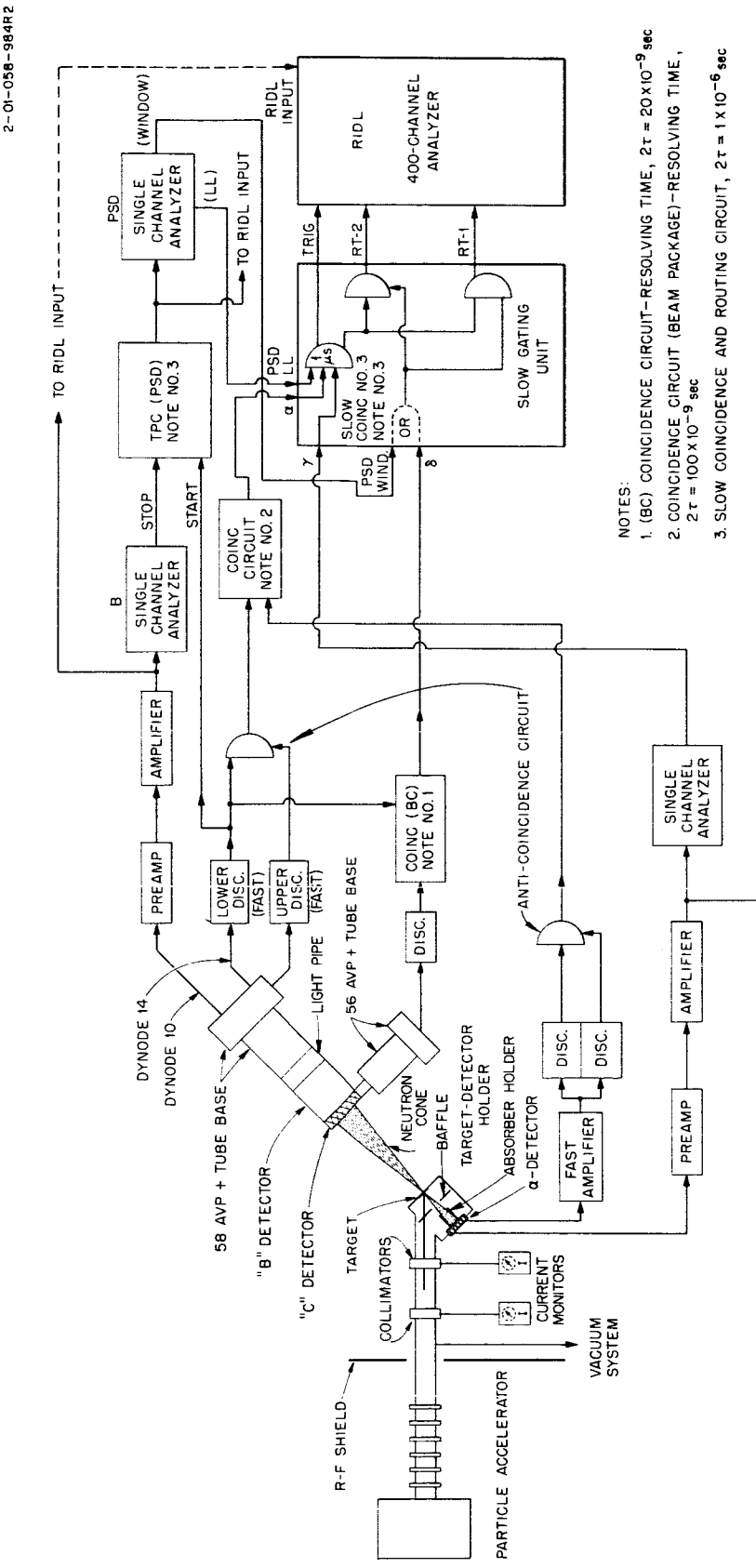

Fig. 1. Block Diagram of Experimental Arrangement and Electronic Circuitry for Measurement of Scintillator Efficiency.

Detectors

The two 12-cm-diam NE-213 neutron detectors, one being 2.61 cm thick (designated as B1) and the other 6.1 cm thick (designated as B2), were each mounted on a 58AVP* photomultiplier tube operated with a negative high voltage of approximately 2200 V. Each NE-213 detector had mounted on its face (optically isolated) a thin NE-102** plastic detector (designated as C) to allow differentiation between incident charged particles and neutrons. These thin detectors were coupled to 56AVP photomultiplier tubes. Incident charged particles with sufficient energy to be detected by detector B would at the same time have given a pulse in C. Suitable anti-coincidence circuitry allowed charged particles to be separated.

The neutron detector was positioned on an arm which rotated about the target. The angle and distance of this detector were varied with respect to the target in order to ensure that every neutron associated with a detected charged particle was intercepted. For most of the experiments these neutrons covered about 25% of the total area of the neutron detector.

The charged-particle detector† was a 200-μ-thick silicon surface-barrier detector having a 50-mm^2 sensitive area. It was constructed from 3200-ohm-cm, n-type silicon and was operated at a bias voltage of 100 V,

---

*The 56AVP is a fast 14-stage high-gain photomultiplier tube provided with a cesium-antimony semitransparent curved cathode having a diameter of 42 mm. The tube is distributed by the Amperex Electronic Corporation.

**NE-102, also manufactured by Nuclear Enterprises, is a plastic scintillator with hydrogen and carbon densities of 5.4 and 4.8 x 10^{22} atoms/g, respectively, and sp gr of 1.035 at 23°C.

†Purchased from Oak Ridge Technical Enterprises Corporation, Oak Ridge, Tennessee, and mounted by R. E. Zedler of the Instrumentation and Controls Division of ORNL.

resulting in full depletion. [The 3.5-MeV proton from the $D(d,p)^3H$ reaction has a range of 100 μ in silicon.] The resolution of the detector was ~30 keV for ~5-MeV alpha particles from a thin source but the energy spread of the particles observed during the experiment was much larger as is shown in Table 2. The detection efficiency was very nearly 100%. This detector was located at an angle of 120° with respect to the deuteron beam and subtended a solid angle of 0.016 steradian. Figure 2 illustrates the spectrum of charged particles in the detector resulting from deuterons striking a target containing both deuterium and tritium; ^3He and ^3H particles were eliminated by an absorber.

Collimation

Final collimation of the incident deuteron beam was accomplished by use of a 10-mil-thick tantalum plate with a 1.5-mm-diam hole, located 10 cm from the target. The target was inclined to the beam at a grazing angle of 30°, as shown in Fig. 1, so that the beam shadow on the target plane was a 1.5 x 3.0 mm ellipse. This spot size was verified by observing a quartz viewer in the target plane. Collimation of the secondary charged particles was accomplished by the sensitive surface of the detector.

Differentiation of Product Charged Particles

In order to separate the charged particles in energy and to prevent detection of deuterons scattered from the target, aluminum or aluminized mylar foils were placed between the target and the detector. In the $D(d,n)^3He$ and $D(d,p)^3H$ reactions, the energies of the ^3He, p, and ^3H particles were differentially reduced. The approximate average energy of the particle at the charged-particle detector is given in Table 2. The thicknesses of the absorbers were nominally 1.43 mg/cm^2 aluminum-equivalent

Table 2. Energies of Outgoing Charged Particles from the $T(d,n)^4He$, $D(d,n)^3He$ and $D(d,p)^3H$ Reactions at Various Positions

(Detector angle with respect to incident beam = 120 deg.)

Reaction	Outgoing Particle	Absorber Thickness (Al equiv.)	Deuteron Energy at Point of Interaction[a] (keV)	Approximate Energy (MeV) of Outgoing Particle		
				At Point of Interaction	At Surface of Target	At Surface of Diode
$T(d,n)^4He$	^4He	250 $\mu g/cm^2$	0	3.51	3.11	2.91
			93	3.28	3.19	2.99
			135	3.20	3.20	3.00
		1.43 mg/cm^2	0	3.51	3.11	-
			93	3.28	3.19	2.04
			135	3.20	3.20	-
$D(d,n)^3He$	^3He	250 $\mu g/cm^2$	0	0.820	0.380	0.115
			62	0.692	0.626	0.354
			85	0.657	0.657	0.382
$D(d,p)^3H$	^3H	250 $\mu g/cm^2$	0	1.010	0.898	0.826
			62	0.854	0.837	0.762
			85	0.857	0.827	0.752
	p	250 $\mu g/cm^2$	0	3.03	2.98	2.96
			93	2.88	2.87	2.85
			135	2.86	2.86	2.84
		1.43 mg/cm^2	0	3.03	2.98	2.84
			93	2.88	2.87	2.73
			135	2.86	2.86	2.72

a. Maximum energy listed for each reaction is the E_{dmax} energy.

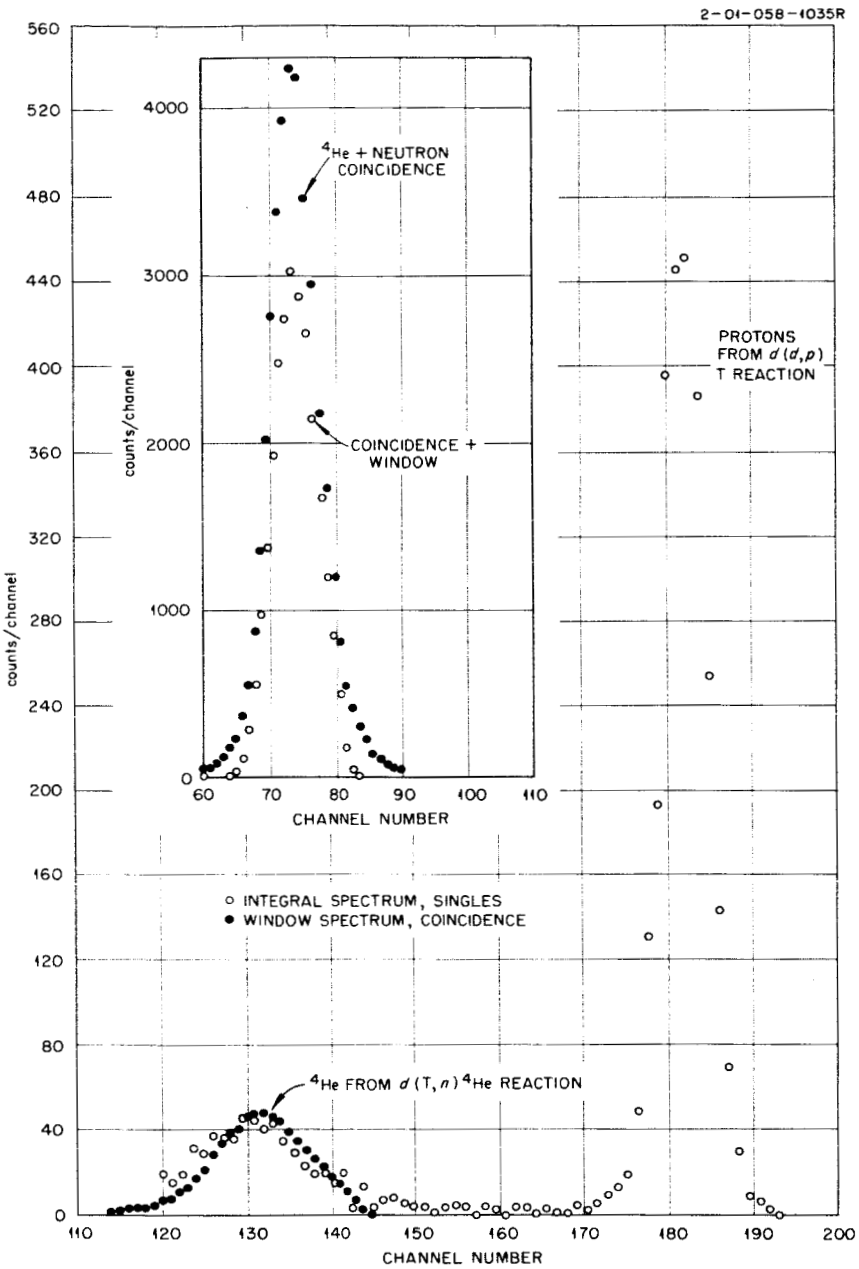

Fig. 2. Pulse-Height Spectra from the Charged Particle Detector for Incident 135-keV Deuterons with a 1.43-mg/cm^2 Al Equivalent Absorber Between the Tritium Target and the 200-μ Solid-State Detector. Note that zero is suppressed for abcissa values.

for the measurements using the $T(d,n)^4He$ reaction and 250 $\mu g/cm^2$ for those using the $D(d,n)^3He$ reactions.*

During the experiments using the $D(d,n)^3He$ reaction, a window was set across the peak in the pulse-height distribution caused by the ^3He particles. Similarly a window was set across the peak in the pulse-height distribution of the ^4He particles from the $T(d,n)^4He$ reaction. In both cases the apparent efficiency was measured as a function of window position and width. Subsequently, the window position and width were adjusted to fall within the regions which gave constant efficiency within the statistical error. This procedure ensured that only the proper associated particle was counted. Figures 2 and 3 show the charged-particle spectra from the solid-state detector for the $D(T,n)^4He$ and the $D(d,n)^3He$ reactions, respectively, with and without a discriminator window. The spectrum with the window was taken in coincidence with the pulses from the NE-213 detector. The very large number of protons illustrated in Fig. 2 were observed from a target having only a small amount of tritium and a large amount of deuterium. This target was chosen in order to make apparent the protons from the $D(d,p)^3H$ reaction.

*A thinner "dE/dx" solid-state detector may be used to ease discrimination between ^4He particles and the background protons, since in this case the protons give relatively small pulses. The dimension of such a detector is dictated by the maximum range of the alpha particle. A 40-μ-thick detector was used successfully in this manner, with the advantage that only a single discriminator was required to isolate the desired alpha particles. With such a thin counter the T(d,n) reaction may be studied using an ~500-$\mu g/cm^2$-thick absorber to stop the scattered deuterons.

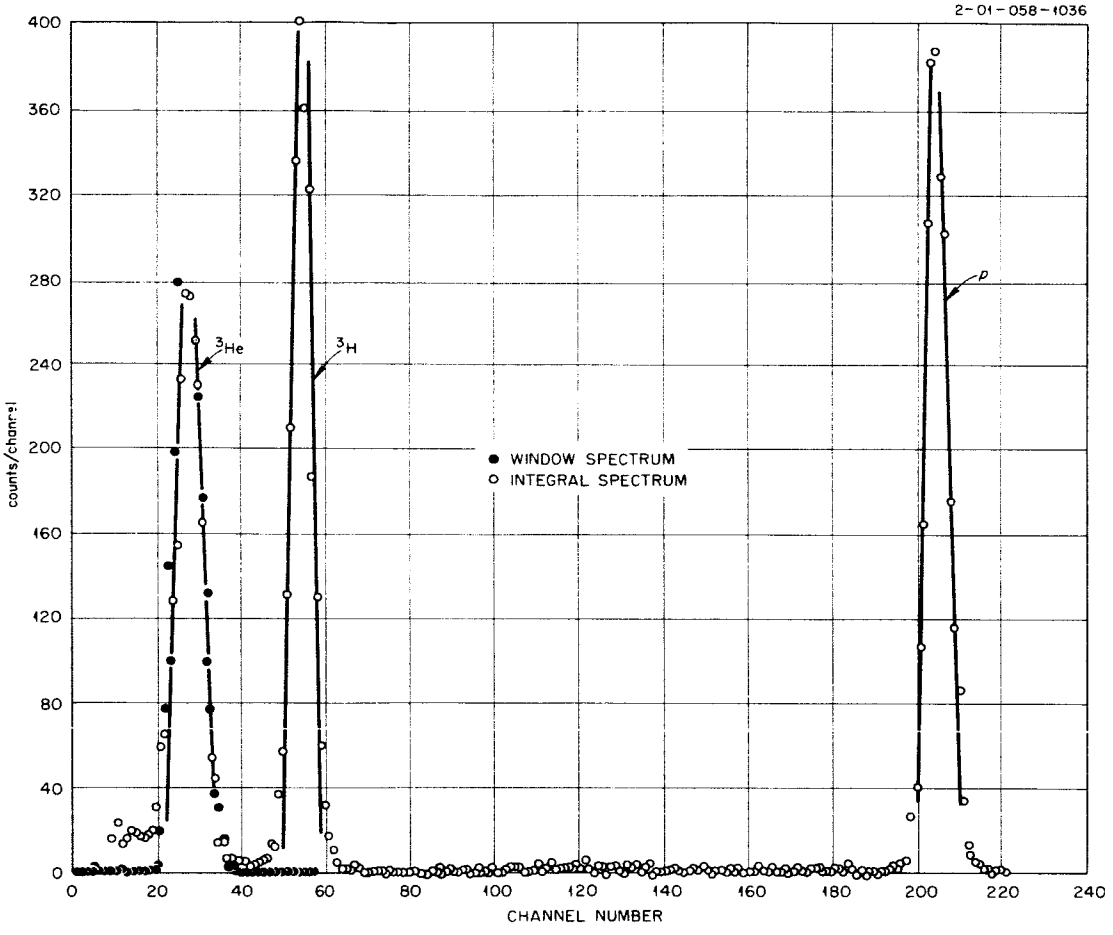

Fig. 3. Pulse-Height Spectra from the Charged Particle Detector for Incident 85-keV Deuterons with a 250-$\mu g/cm^2$ Al Absorber Between the Deuterium Target and the 200-μ Solid-State Detector. The window spectrum is in coincidence with detector B.

IV. ELECTRONICS

Associated Particle System

A charged particle incident upon the solid-state detector produced a pulse which was amplified by a fast amplifier as shown in Fig. 1. The pulse from this amplifier had a rise time of ~4 nsec and a length of about the same duration.[9] The output signal from the amplifier was fed in parallel to two tunnel diode univibrator discriminators which were set to establish a window across the peak in the pulse-height spectrum. The output signal from this window was fed into a coincidence circuit.

The solid-state detector also fed an integrated pulse through a slow preamplifier and amplifier to a multichannel analyzer for observation of the charged-particle pulse-height spectrum. The output of the slow amplifier was also fed into a single-channel analyzer to determine a range of acceptable pulse-heights. During part of these experiments this circuit was used to establish a window instead of the two fast discriminators mentioned above. This arrangement bypassed the fast coincidence circuit, the effect of which was to lengthen the coincidence resolving time.

Neutron Detector System

Pulses (~4-nsec rise time and 10-nsec full-width at half maximum) arising from detection of radiation in the neutron detector were similarly fed into a fast tunnel diode discriminator, the output of which went into a coincidence circuit. The threshold of this discriminator always determined the neutron counting efficiency. (Since two discriminators were available, a few measurements were made with one discriminator in anti-coincidence with the other in order to observe the efficiency within discrete proton recoil energy ranges.)

The coincidence circuits established a coincidence in time between pulses from the charged-particle detector and the neutron detector. The time resolution was ~100 nsec. The output of this circuit was fed into a slow (1.2-μsec) coincidence and routing circuit.

Output of the neutron detector was also integrated and fed into a slow preamplifier and amplifier (0.7-μsec clipping time). The output of the slow amplifier was used to feed a multichannel analyzer which recorded the pulse-height spectrum.

Pulse-Shape Discrimination

NE-213 was designed for optimum difference in shape between pulses caused by heavy particles (protons, alphas) and by gamma rays. The fast component of light intensity has a very fast rise time, and the output pulse rise time is governed by the photomultiplier tube. The decay time of the fast component is ~3 nsec to 1/e. The slow component is not a pure exponential but has a time constant of the order of tenths of microseconds. The method of pulse-shape discrimination (PSD) used here depends on the pulse-shape dependence of the zero crossover point of a bipolar pulse from a standard double-delay-line linear amplifier. This use of the crossover timing was described by Forte,[10] and the system used here has been described elsewhere.[11]

As shown on the block diagram, this amplifier is fed by the usual charge pulse from dynode 11 of the photomultiplier tube. In order to make use of differences in pulse crossover timing, the event in the phosphor is timed by the fast discriminator on detector B. An output of this discriminator gives a "start" pulse to a time-to-pulse-height converter (TPC). The discriminator is set to accept a pulse arising from the fast component

of light appearing at dynode 14 of the photomultiplier tube. Amplitude of the output of the TPC is controlled by a "stop" pulse from the crossover-pickoff detector, which varies in time according to the ratio of the slow-to-fast-light components. The "stop" pulse is generated by the "B" crossover-pickoff single-channel analyzer which had its lower level always set below that of the fast discriminator operating on the current pulse from dynode 14. The output of the TPC thus has two groups of pulses separated in amplitude by an amount linearly dependent upon the timing of the crossover point of the output of the amplifier. There is of course an indeterminate region due to the time slewing of the start pulse and the jitter and time slewing of the crossover-pickoff circuit. The relative excess of the slow decay light component from a heavy particle will result in a crossover delay of about 10-30 nsec relative to the crossover from a gamma ray, depending on the time constants of the amplifier and the energy of the heavy particle. A time distribution of pulses at the output of the TPC using a Po-Be source near the detector is shown in Fig. 4. An amplifier with output rise time of about 1 μsec was used to amplify the output pulses of the TPC before they were fed into the multichannel analyzer.

As the energy of the recoil proton increased, the slow-to-fast ratio of light given off approached that of an electron and therefore the ability to differentiate gamma rays (electrons) from protons decreased. For this reason and for the reason that there is gross time slewing when the amplifier is overloaded, the upper level of the single-channel analyzer was set to fire at pulse heights corresponding to pulses generated by gamma rays greater than ~2 MeV. Protons giving rise to similar pulse heights were of energies of about 5 or 6 MeV. None of the pulses above this threshold provided a stop pulse to the TPC and therefore the corresponding events were all treated as proton recoils.

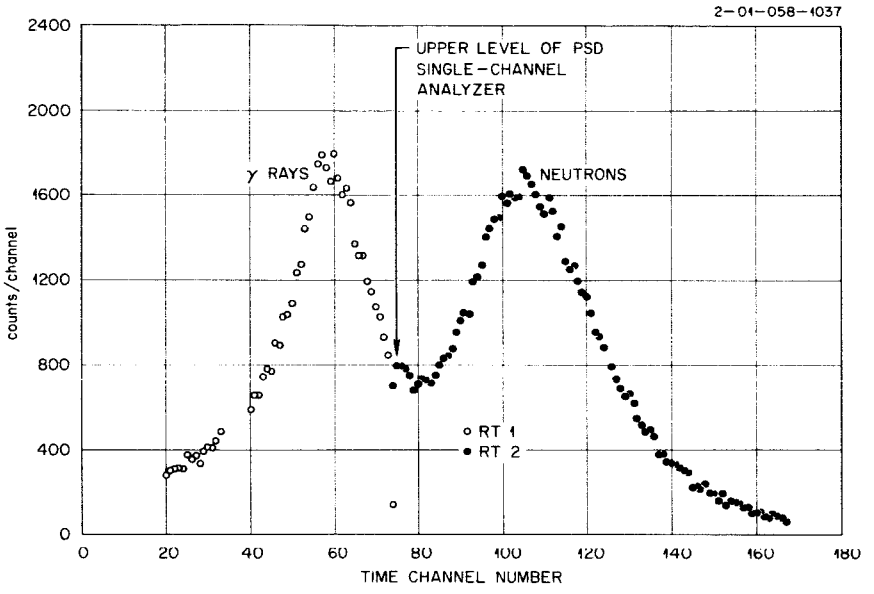

Fig. 4. Time Distribution of Pulses as Observed at the Output of the Time-to-Amplitude Converter as Employed for PSD. The source is Po-Be; each channel corresponds to 0.4 nsec.

The output of the TPC was examined by an ordinary single-channel analyzer (PHA) to make a final identification of each event. The lower-level output and the output of the window were fed into the slow coincidence and routing circuit. The window was set over that range of pulse amplitudes corresponding to gamma rays. As shown in Fig. 4, the upper level was set slightly below the minimum point in the time distribution curve to ensure that few neutrons were miscalled gamma rays.

Coincidence circuit No. 3, the slow coincidence and routing circuit, provided an announcement that all predetermined conditions had been met and it determined in which half of the analyzer a pulse was to be stored. The second half of the analyzer was chosen for the storage of signals which met the criteria established for neutrons, while the first half stored all others. A coincidence between pulses from C and pulses from B (time resolution was about 20 nsec) (both in coincidence with the charged-particle output pulse) caused inputs into the multichannel analyzer to be stored in the first half. Pulses from the window of the TPC single channel analyzer also routed signals to the first half. All bias adjustments were made such that the lower level discriminator on the neutron detector preempted. This bias was controlled by adjustment of the current through a fast tunnel diode driven by the current pulse from dynode 14 of the photomultiplier tube. Since this is a very fast pulse, bias settings were made by observation on the multichannel analyzer of pulse heights from incident gamma rays, as gated by the fast discriminator. For a given amplitude fast signal as measured by the fast discriminator, the neutron-associated pulse from the slow amplifier has a larger (about 50% at 200-keV electron energy) amplitude than the gamma-ray pulse because of the relatively greater slow

component which accompanies the heavy-particle pulses. For a given light output from the detector, the electron pulse required much less energy than the heavy-particle one, the factor being about six for 1-MeV neutrons. Thus a threshold bias operating on the fast portion of the light from an incident gamma-ray-produced electron of about 170 keV would correspond to a neutron threshold of ~1 MeV.

V. EXPERIMENTAL PROCEDURE

At the start of the experiments the pulses from the photomultiplier tubes were observed using Model No. 519 and 561 Tektronix oscilloscopes. The focusing and accelerating voltages of the photomultiplier tubes were adjusted to give minimum rise time of the fast pulses and minimum distortion of pulse shapes at overload. Peak currents were ~60 ma, well within the advertised limit (1 amp) of the 58AVP. Count rates were kept to about 2000 counts/sec in either detector for pulses whose fast components were above 160-keV electron-equivalent.

In every case the window, which determined acceptance of charged particles, was varied both in width and position over the pulse-height spectrum from the solid-state detector to ensure uniqueness of association with the neutrons of interest.

Resolving times of all coincidence circuits were measured and adjusted to give 100% efficiency and still have few random counts present. As stated earlier the neutron detector was placed on an arm which rotated about the target. Figure 5 shows a plot of apparent efficiency vs angle with respect to the incoming deuterons, as well as apparent efficiency vs the distance of the neutron detector from the target for the case of 14.4-MeV neutrons. The final detector B position for the 14.4-MeV neutron

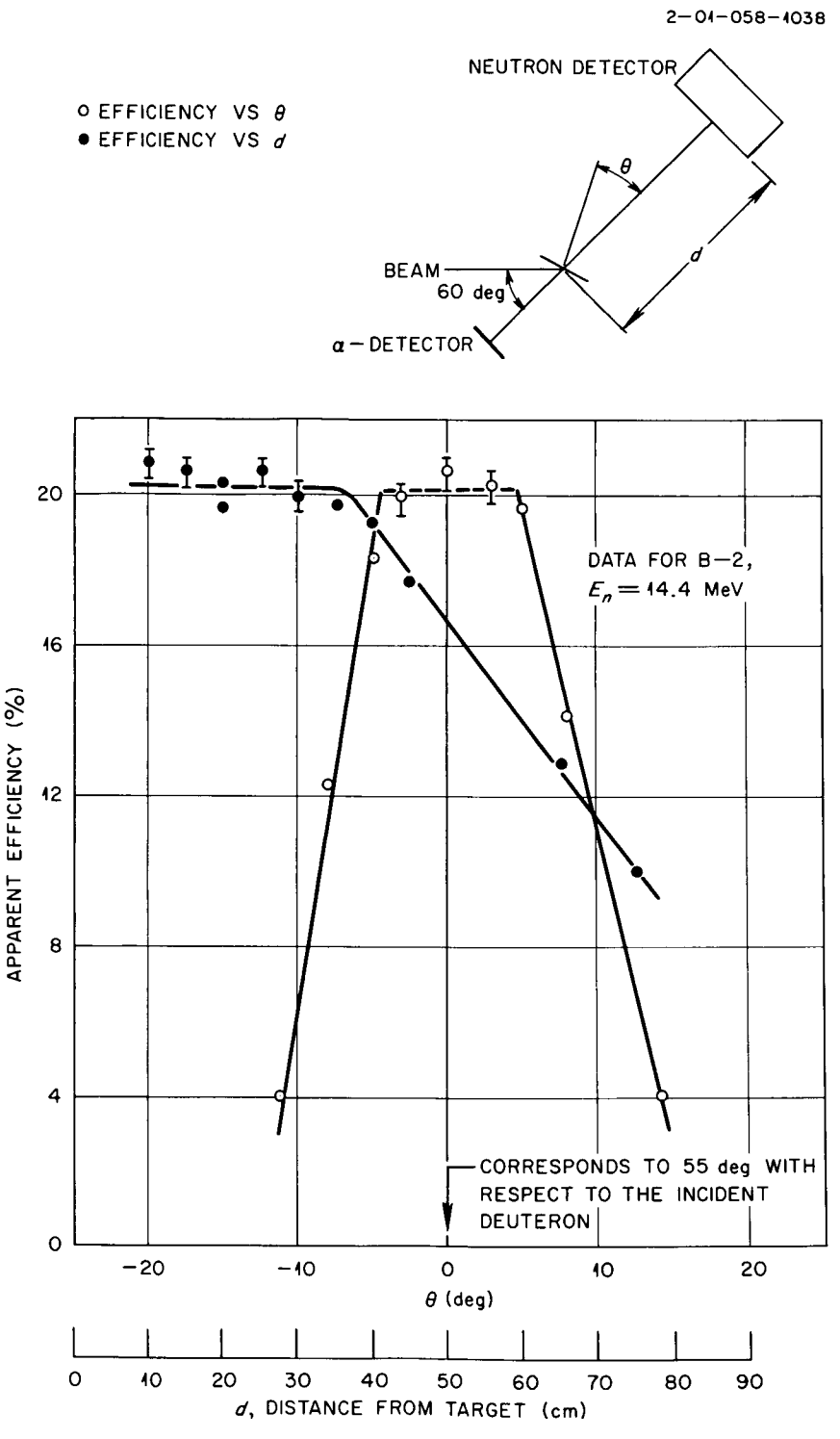

Fig. 5. Ratio of Coincidence Counts to Charged-Particle Counts Plotted as a Function of Angle, θ, and Distance, d, for a 12-cm-diam Neutron Detector.

experiments was typically chosen to be 25 cm from the target, at an angle of 55° with respect to the deuteron beam. This position is in agreement with the calculated value from Blumberg and Schlesinger.[12] Similar tests made for the $D(d,n)^3He$ case placed the detector at the correct angle and distance.

VI. DISCUSSION AND RESULTS

Energy Checks by Time-of-Flight Techniques

A time spectrum using neutron time-of-flight techniques over a 40-cm flight path was used to determine whether or not events giving counts routed into the first half of the analyzer were the same time-wise as those routed into the second half. The system had large errors (±2 nsec, ~ ±5 channels). The time spectrum for 14.4-MeV neutrons is shown in Fig. 6. Also shown is a time spectrum where the bias was raised to ~2-MeV electron-equivalent measured with a ThC" source. Examination of the flight-time spectra, the pulse-height spectra, and the spurious timing variations (slewing) as a function of pulse height allows an assignment of 99% of the pulses stored in both halves of the analyzer to be related to ~14.4-MeV neutrons that interact in or near the scintillator. The other 1% probably comes from nominal 14.4-MeV neutrons which are scattered by surrounding materials.

Effects of Detector C

An anticoincidence counter, detector C in Fig. 1, was located immediately ahead of detector B. This detector has been used in previous experiments to eliminate counts due to charged particles from measured flight-time spectra, and its design prevented it from being removed for these measurements without damaging detector B. Experimental measurements

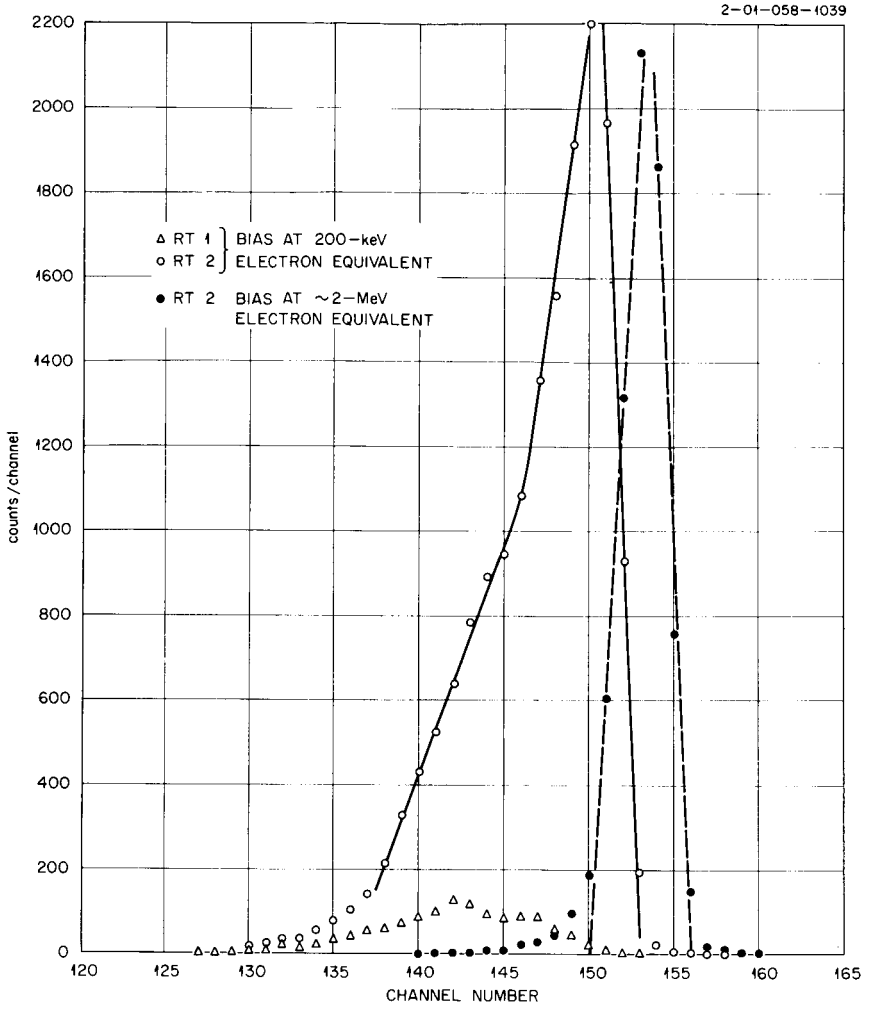

Fig. 6. Time Spectrum for the Approximately 14-MeV Neutrons as Measured at the Output of a Time-to-Amplitude Converter. Each channel is approximately 0.4 nsec. The TPC bias is 90 keV.

determine that the effect on the neutron efficiency of rejecting coincidence with detector C was small, comparable with uncertainties from counting statistics. From simple considerations, detector C can be shown to be a neutron attenuator which moderates a small percent of the neutrons sufficiently so that the detector system responds to a spectrum of slightly reduced intensity and slightly lowered average neutron energy. Monte Carlo calculations were made to estimate the effect of detector C on the efficiency measurements, and the appropriate corrections were introduced.

PSD Effects

Counts stored in RT-1 (see Fig. 1) are a combination of those resulting from BC coincidence, gamma rays of energy below about 2 MeV, and neutrons which are routed due to the imperfect operation of the PSD circuit, all of which must be in coincidence with a pulse from the charged-particle detector and are therefore associated with a neutron passing through the detector. Comparison of the calculated efficiency for the production and detection of the gamma rays from $C(n,n')C^*$ reaction to the measured value of 4.43-MeV gammas shows that at least 50% of the RT-1 counts are due to heavy charged particles from neutron reactions when detector B2 is used, and at least 75% when detector B1 is used. There are two mechanisms which allow this to happen, the most important of which is the timing jitter of the pulse crossover point. This jitter is serious for the lower proton recoil energies. The other mechanism involves proton recoils which lose energy in the detector during the early part of the slowing-down process and then escape from the sensitive volume. (For 14.4-MeV neutrons, about 3% of the RT-1 counts are due to this process when detector B1 is used and 1% when

detector B2 is used. These numbers are for the "standard" condition, i.e., a 160-keV counting threshold and a PSD threshold such that all pulses greater than 2-MeV electron-equivalent are declared to be caused by neutrons.)

The sensitivity of the number of RT-2 counts to the setting of the upper level PSD discriminator was measured over about 10 channels in the valley of the PSD curve shown in Fig. 4. The effect on the number of counts was about 0.5% per channel variation in the upper PSD setting.

Bias Determination

Since the B-detector system is not noise-free, the measurements had to be made in terms of the efficiencies above some bias level. Several values of bias were used for these data, and in every case they were determined by the settings of the circuitry pertinent to the detector. Bias settings in terms of energy are always referred to the pulse height produced by Compton electrons from well-known gamma-ray sources. Discriminators operated on the fast portion of the pulse, and the corresponding total light was recorded.

In order to establish the value of the fast univibrator threshold in terms of electron energy, a monoenergetic gamma-ray source was used to obtain a pulse-height spectrum of total light outputs from those recoil electron events that produced enough fast light to trigger the fast discriminator. For each threshold setting the gamma-ray energy was chosen to produce Compton electrons having as little energy above the threshold as practicable. These gated pulse-height distributions were interpreted by performing an approximate calculation to fit the observed spectrum in terms of the threshold electron energy. The electron-energy-loss distribution was first estimated by using the Monte Carlo code of Zerby and Moran[13]

in the case of the 393-keV gamma ray of ^{113}Sn, or in other cases by an approximate third-order scattering model for axial incidence on a disc scintillator. These energy-loss distributions show definite contributions for absorbed energies greater than the Compton edge, though the detector resolution prevented these contributions from being obvious in the pulse-height spectrum. To allow for the finite resolution, the energy-loss density function was folded with a normal density function having the same standard deviation as a Poisson function with mean ke, where e is the absorbed electron energy (keV) and k is the number of "effective" photoelectrons/keV. The fast threshold was included by assuming that a fitted fraction δ of the light from an event (δke photoelectrons) was effective in influencing the fast discriminator. The inclusion of the resulting statistical effects in the threshold region allowed the calculation to approximate the shapes of gated total light pulse-height spectra as shown in Fig. 7. The drawbacks of the calibration scheme were that nonlinear light production by electrons at low energies, electron escape, and the light transfer variance were ignored, though all can be shown to be important. In the case of the transfer variance this resulted in the need to choose a different value of k for each source energy. Using fits of the type shown in Fig. 7, it was usually possible to estimate thresholds with a reproducibility of better than 5%.

Figure 7 shows the calibration spectra used to determine the bias for a typical efficiency measurement. The measured pulse-height spectra do not quite fit any calculated spectrum, but the uncertainty in determining the cut-off energy is ±5 keV, assuming that the same criteria are used in every case. For these measurements, the energy corresponding to the intersection of the

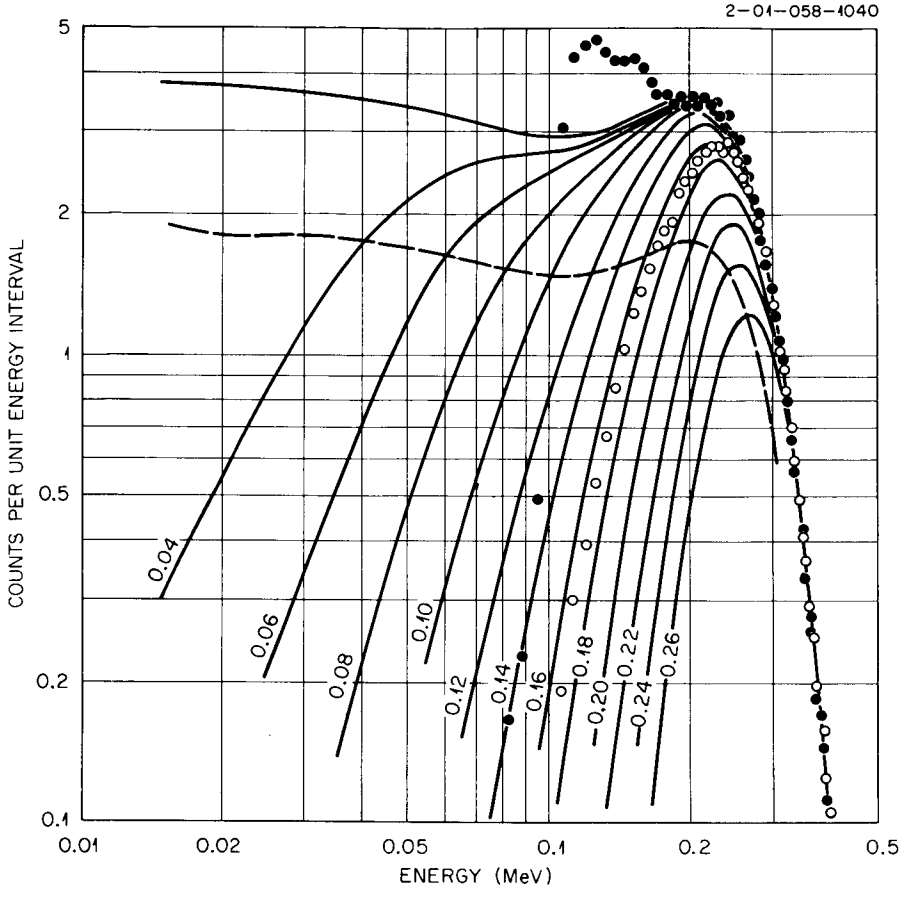

Fig. 7. Experimental and Calculated Pulse-Height Responses of 6.1-cm-thick Detector for Incident 0.393-MeV Gamma Rays (100 photoelectrons/MeV, $\delta = 0.40$). — calculated pulse-height response for various bias values, -- half-amplitude of integral pulse-height curve, ● measured pulse-height response for very low total light bias, no fast threshold, and ⊙ measured pulse-height response for 165-keV cutoff.

lower cutoff of the measured pulse-height spectrum and the curve representing 0.5 of the calculated curve, after the magnitudes of the spectral intensities had been normalized at higher pulse heights, was defined as the bias point. This criterion was chosen because observations showed that the calculated bias cutoff and the measured pulse-height curve intercepted at the half-value of the calculated pulse-height distribution curve for a wide range of bias values independent of the value of δ used in the calculations.

The gain of the system was checked before and after each run using a ^{113}Sn source. However, over the range of electron energy from ~0.3 to ~4.2 MeV, an ~10% nonlinearity was observed. For this reason, when an efficiency is listed for a given bias the gamma-ray source used to determine the bias is also specified.

Figure 8 shows a typical uncorrected pulse-height spectrum for incident ~14.4-MeV neutrons for scintillator B2 biased at 160 keV. The sharp rise at the lower end of both the RT-1 and the RT-2 curves is evidence of the increasing importance of the nonelastic cross section for the $^{12}C(n,\alpha)$ reactions as well as the poor operation of the PSD circuits for very low pulse heights. The sharp upper cutoff in the RT-1 spectrum results from the setting of the upper level discriminator on the detector output. Counts above this cutoff in RT-1 are routed by the BC coincidence circuit.

Results

Table 3 gives the results of the measurements for both detectors as a function of the bias determined by the fast light. The column labeled ϵ_T is the measured value for the efficiency corrected for background and dead

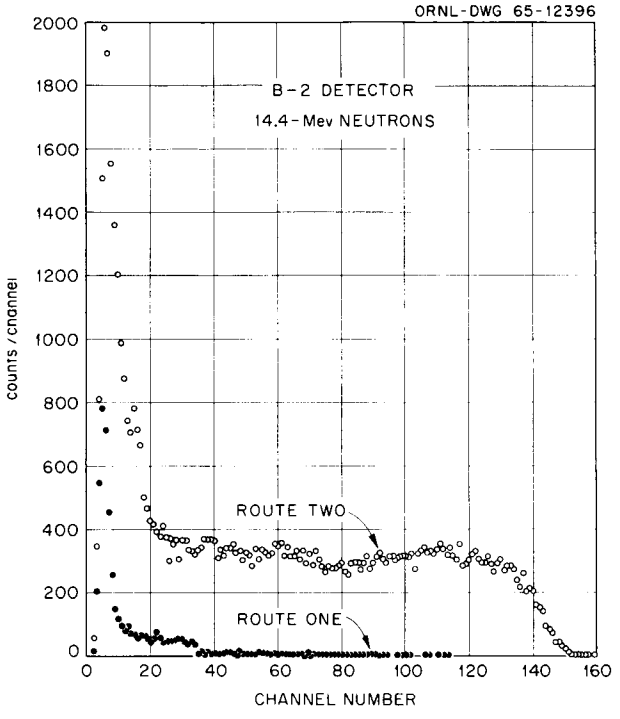

Fig. 8. Typical Pulse-Height Spectra for a 6.10-cm-thick Detector for Incident 14.4-MeV Neutrons.

time. ϵ_T includes the corrections for multiple scattering of the charged particles in passage through the absorber and target. For the $T(d,n)^4He$ reaction, the rms scattering angle for the ^4He particle is $\sim 1^o$. In all configurations of target and detector, except the case of detector B1 at 14.4 MeV, these corrections for ϵ_T were negligible. In the exception, detector B1 was positioned sufficiently far from the target that multiply scattered charged particles could enter detector A with no corresponding conjugate neutrons striking detector B.[14] As a result, the measured efficiency was too low by a factor of 1.005. The effect of the pulse-shape discrimination circuits are demonstrated by the ϵ_{RT-1} and ϵ_{RT-2} columns where ϵ_{RT-1} is the number of counts routed into the first half of the analyzer divided by the total alpha counts and ϵ_{RT-2} is the number of counts routed into the second half of the analyzer divided by the total alpha counts. The last two columns in the table show the effects of detector C and the light pipe using correction values obtained from an O5R Monte Carlo calculation.[15] Uncertainties in these corrected values are large because of ~1-2% Monte Carlo statistical effects.

Figure 9 gives plots of integral efficiency vs bias for both detectors with points calculated by Schuttler[16] shown for comparison. The ϵ_T values are used since Schuttler's calculation corresponds to the case without pulse-shape discrimination. Comparison with other work is difficult because the distinction between "fast" and total light is usually ignored and in many cases the bias is mentioned only in terms of light produced by neutrons. Perey's[7] measurements for a 5-cm-thick plastic scintillator normalized for density are comparable with detector B2. He reports an efficiency of 0.20 ± 0.01 for 14-MeV neutrons using a bias level equal to

Table 3. Efficiencies of 2.61- and 6.10-cm-thick Scintillators for Detecting 14.4- and 2.66-MeV Neutrons

(The measured total efficiency, ϵ_T, is given as a function of the bias energy obtained from the fast light. Comparison is made with the RT-1 and RT-2 efficiency values obtained through the use of the pulse-shape discriminator. The data are corrected for instrument dead time and background. In the case of the B1 detector and 14.4-MeV neutrons, the data are also corrected for multiple scattering.)

Source	No. of Measurements	Bias (keV)	ϵ_T (%)	ϵ_{RT-1} (%)	ϵ_{RT-2} (%)	$\epsilon_{(RT-1)+(RT-2)}$ (%)	ϵ_T Corrected[a] For C (%)	ϵ_T Corrected[b] For LP + C (%)
			Detector B1 (2.61 cm), E_n = 14.4 MeV					
^{113}Sn	1	118 ± 5[c]	11.29 ± .06	0.88 ± .009	10.33 ± .10	11.21 ± .10	11.23	10.96
	3	130 ± 5[c]	11.22 ± .08	0.86 ± .020	10.33 ± .10	11.19 ± .10	11.16	10.89
	2	160 ± 5[c]	10.97 ± .07	0.84 ± .02	10.24 ± .10	11.08 ± .10	10.92	10.65
	2	165 ± 5[c]	10.65 ± .08	0.78 ± .02	9.89 ± .10	10.67 ± .10	10.60	10.34
	3	195 ± 5[c,d]	10.60 ± .08	0.77 ± .02	9.79 ± .10	10.55 ± .10	10.55	10.33
	1	200 ± 5	10.48 ± .07	0.82 ± .01	9.63 ± .05	10.44 ± .06	10.43	10.17
^{60}Co	1	766 ± 5	7.44 ± .05	0.28 ± .007	7.17 ± .05	7.45 ± .05	7.44	7.22
ThC''	1	1800 ± 50	5.67 ± .05	0.08 ± .004	5.59 ± .05	5.67 ± .05	5.65	5.56
Po-Be	1	3700 ± 100	4.48 ± .04	0.03 ± .003	4.44 ± .05	4.47 ± .05	4.46	4.37
			Detector B1 (2.61 cm), E_n = 2.66 MeV					
^{113}Sn		120 ± 5	19.44 ± .11	1.29 ± .02	18.15 ± .10	19.44 ± .11	18.49	19.27
		160 ± 5	17.70 ± .11	1.05 ± .02	16.65 ± .10	17.70 ± .10	16.83	17.54
		200 ± 5	16.75 ± .10	4.36 ± .05	12.38 ± .09	16.75 ± .10	15.93	16.60
		207 ± 5	16.38 ± .10	0.59 ± .02	15.79 ± .10	16.38 ± .10	15.57	16.23

		Detector B2 (6.10-cm), E_n = 14.4 MeV						
^{113}Sn	1	120 ± 5[c]	24.16 ± .13	2.02 ± .06	22.14 ± .22	24.16 ± .23	24.16	23.67
	1	127 ± 5	24.46 ± .24	2.12 ± .07	22.26 ± .24	24.38 ± .25	24.46	23.96
	1	140 ± 5[c]	23.81 ± .07	1.99 ± .09	21.65 ± .21	23.64 ± .23	23.81	23.34
	1	160 ± 5[c]	23.42 ± .06	2.00 ± .09	21.52 ± .21	23.52 ± .23	23.42	23.14
	5	170 ± 5[c,e]	23.30 ± .09	1.82 ± .09	21.39 ± .21	23.21 ± .23	23.30	22.85
	1	180 ± 5	23.04 ± .30	1.80 ± .02	21.10 ± .09	22.90 ± .10	23.04	22.61
	1	200 ± 5[c]	22.58 ± .08	1.74 ± .09	20.88 ± .20	22.62 ± .22	22.58	22.16
	1	255 ± 10	21.22 ± .09	1.41 ± .02	19.78 ± .10	21.19 ± .11	21.22	20.82
^{60}Co	1	812 ± 10	16.11 ± .08	0.54 ± .01	15.56 ± .08	16.11 ± .08	16.11	15.87
ThC''	1	2150 ± 50	11.94 ± .06	0.13 ± .007	11.79 ± .06	11.93 ± .06	11.94	11.94
Po-Be	1	3700 ± 100	8.58 ± .07	0.05 ± .001	8.51 ± .07	8.57 ± .07	8.58	8.54
		Detector B2 (6.10 cm), E_n = 2.66 MeV						
^{113}Sn		110 ± 5	39.35 ± .16	2.31 ± .03	37.04 ± .16	39.35 ± .16	37.39	38.54
		200 ± 5	33.68 ± .14	1.70 ± .03	31.97 ± .13	33.68 ± .14	31.72	33.39

a. The correction used is taken from the Monte Carlo data. For E_n = 14.4 MeV, the attenuation by C is minimal. For E_n = 2.66 MeV, C increases the efficiency of the system by nominally 5%.

b. The combined effect of the light pipe and C increases the efficiency by nominally 1.02 ± 0.01 up to ~1 MeV and by 1.00 ± 0.01 above 1 MeV. These corrections are also determined from the Monto Carlo code.

c. For these runs the differential efficiency was recorded only between the stated threshold bias and and ~2 MeV electron total light. Values for the RT-1 and RT-2 efficiencies are corrected to include the efficiency above this cutoff. The uncertainty in the (RT-1) + (RT-2) efficiency is estimated at 1% from dead time calculations.

d. In one of these runs the entire differential efficiency was recorded above the stated bias. The other two (recorded only to ~2 MeV) were corrected for efficiency above ~2 MeV and all three were averaged to give the values tabulated. Errors in the RT-1 and RT-2 efficiencies are due to the uncertainty in the knowledge of the dead time associated with the routing circuitry and the analyzer.

e. The values given are averages of five runs. In two of these runs, the upper cutoff was at ~2 MeV. The uncertainty in (RT-1) + (RT-2) is ~1%.

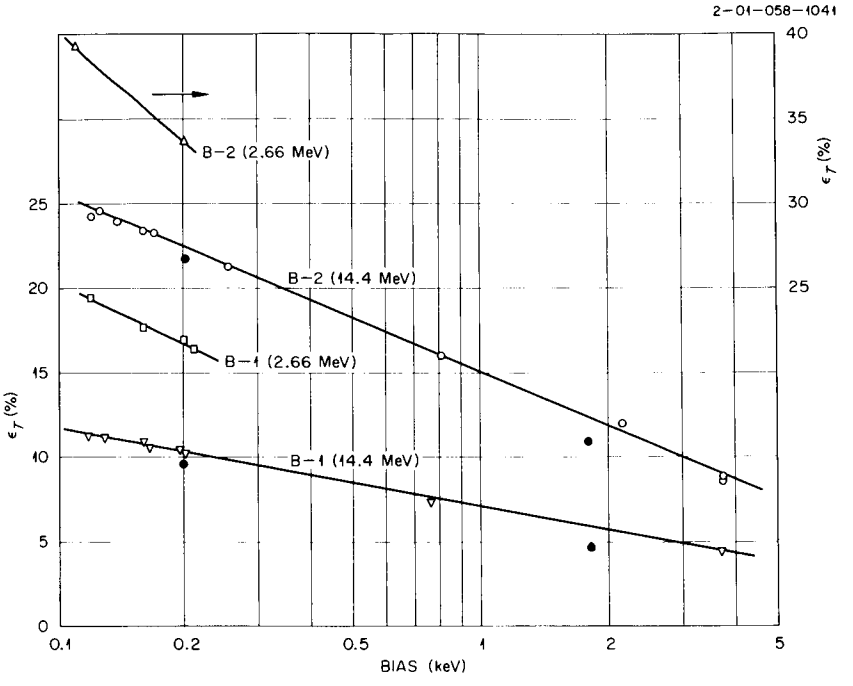

Fig. 9. Total Integral Efficiency as a Function of Fast Bias in Terms of Electron Equivalent Energy. Points labeled ● are those calculated by Schuttler.

the upper edge of the Compton electron spectra from a ^{137}Cs source. Since total light was used, this corresponds to approximately 400-keV fast bias. Perey quotes Bostrom[17] et al. as having reported an efficiency of 0.18 under the same conditions. For this threshold an efficiency of 0.18 is interpolated from Fig. 9.

Hardy[3] gives a semiempirical equation checked at a neutron energy of 2.07 MeV with a bias corresponding to the pulse height produced by a 1-MeV neutron (170-keV electron fast light equivalent). Employing this equation for neutrons of energy 2.66 MeV and using the same bias, one may estimate an efficiency of 0.28 ± 0.02 for a 5-cm-thick NE-213 detector. Correcting this value for self-absorption implies an efficiency of 0.32 for a 6.1-cm-thick detector. From Fig. 9, the comparable efficiency is 0.35.

The differential efficiency as a function of total light output was compared with values obtained analytically using an adaptation of the 05R Monte Carlo code.[18,*] The 05R is an analog Monte Carlo code that provides accurate representation of the cross sections. Neutron histories were individually developed and traced until the neutron escaped, was absorbed, or was reduced in energy to 20 keV or lower. The efficiency was calculated for a normally incident neutron beam with histories being generated until 25,000 light-producing events were recorded. The output of the 05R code was smeared with a Gaussian function so designed that the upper cutoff of the spectrum was fitted to the measured pulse-height curve. The calculated spectrum and efficiency values were obtained for the detector in combination with detector C and the light piper.

*Modifications to the 05R code were made by R. E. Textor, Oak Ridge Gaseous Diffusion Plant.

The cross sections for scattering of neutrons by hydrogen were taken from BNL-325 and those for scattering by carbon from the NDA Library.[19] For a neutron energy of 14.4-MeV E_n, the (n,γ), (n,p) and (n,pn) cross sections for carbon become important. These cross sections and their contributions to the response function are discussed by Verbinski et al.[20] Measured and calculated responses were normalized to the light output of a ^{60}Co source.

Figures 10 and 11 show both measured and calculated differential efficiencies for detectors B1 and B2. Also shown is the response of the detector to a ^{60}Co source. The 1 MeV total light point is derived from a measurement and calculation of ^{60}Co-induced electrons similar to that shown in Fig. 7. This point serves to calibrate the magnitude of the light unit employed in the graphs. The ordinates of Figs. 10 and 11 are absolute values, i.e., there was no normalization of the amplitude of the efficiencies. The roll off at the lower pulse heights is due to the threshold bias and no comparison should be made below these points. Figure 12 is a plot of the integral efficiency from the data shown in Figs. 10 and 11. The 2-4% lack of agreement between the measured and calculated efficiencies is presently assigned to uncertainties in the carbon cross sections used in the calculations and in the light output vs particle energy. Note that the experimental values are generally higher than the calculated ones, while the possible systematic errors would have produced a discrepancy of the opposite sign. In the case of 14.4-MeV neutrons, the neglect in the measurements at low biases of gamma rays produced by inelastic scattering accounts for an efficiency difference of 0.002 between the experimental and

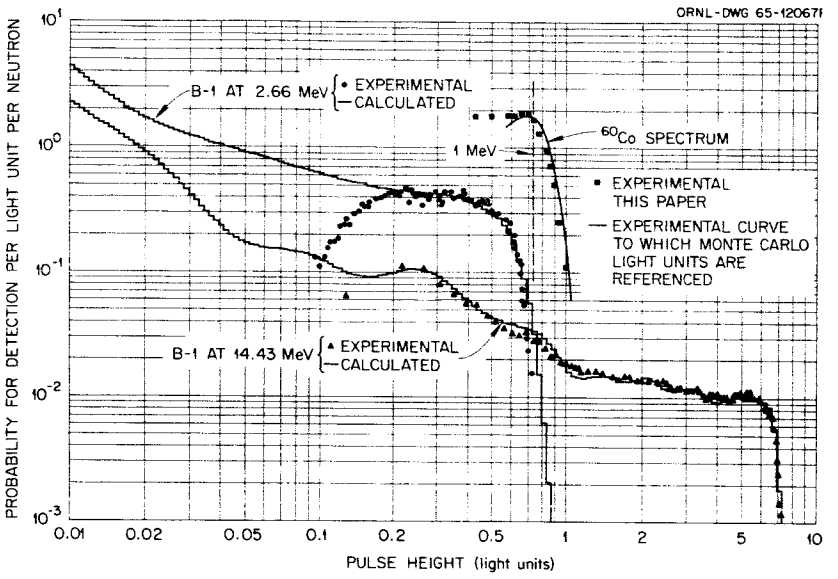

Fig. 10. Differential Efficiency vs Pulse Height in Light Units for a 2.61-cm-thick Detector (B1) for 2.66- and 14.4-MeV Neutrons.

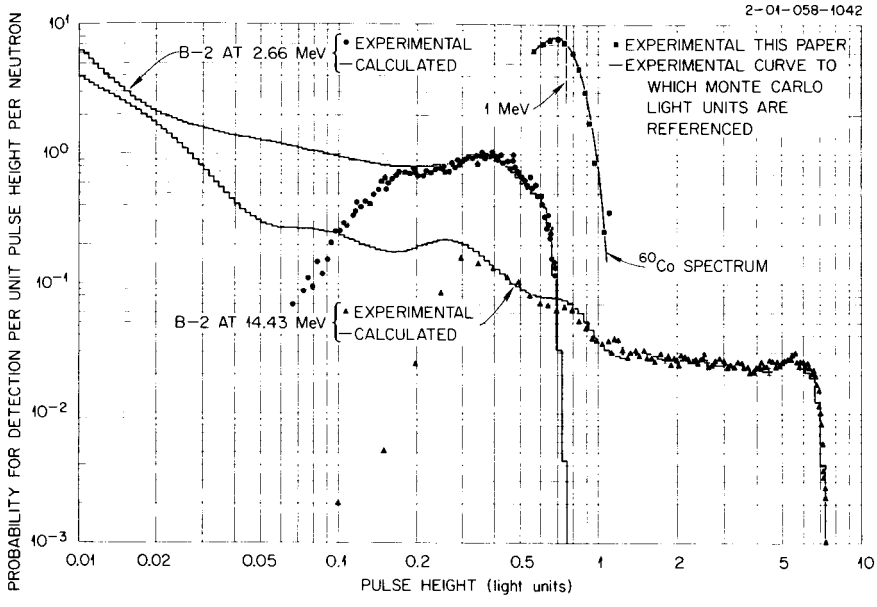

Fig. 11. Differential Efficiency vs Pulse Height in Light Units for a 6.10-cm-thick Detector (B2) for 2.66- and 14.4-MeV Neutrons.

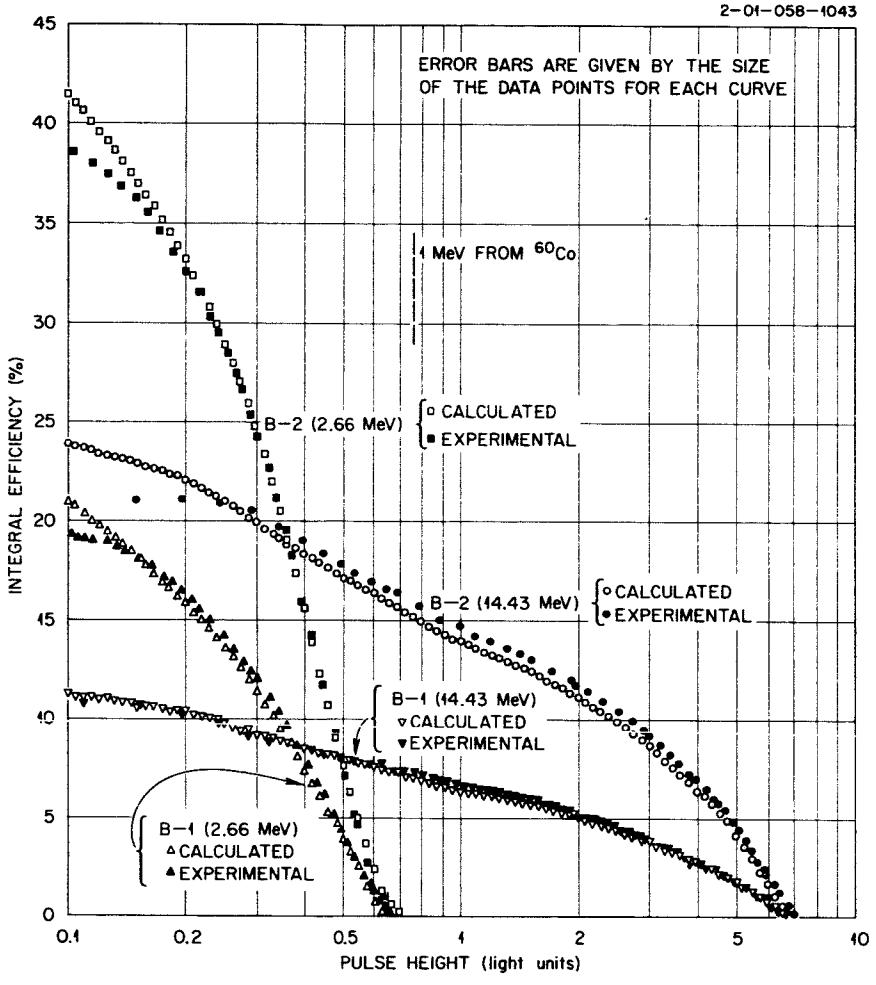

Fig. 12. Integral Efficiency Curves for Detectors B1 and B2 vs Pulse Height in Total Light Units.

the calculated values for the thin detector and 0.006 for the thick detector (about 3% of the ϵ_T values). (Comparison of an efficiency of 0.194 at a bias of 400 keV with the value of 0.183 shown for this bias in Fig. 9 demonstrates the difference between efficiencies measured using fast and total light threshold calibrations.)

Chi-square consistency checks on the integral efficiency covering the total light spectrum above 2.0 MeV (typically, about half the counts), without pulse-shape discrimination, were performed for four runs with detector B2 and eight runs with detector B1. In the case of the thick scintillator, the runs were consistent ($\chi^2/\nu = 1.49$, $P = 0.2$) if a threshold uncertainty of $\frac{1}{2}$ channel was combined with the statistical uncertainties which averaged about 1%. For the case of the thin scintillator, the efficiencies were inconsistent assuming the $\frac{1}{2}$-channel threshold uncertainty ($\chi^2/\nu = 2.6$, $P = 0.01$). The inconsistency suggests that the uncertainties quoted in Table 3 are too small by a factor of about 1.5, though an unexplained uncertainty of one channel in the choice of the threshold would be enough to make the data seem consistent. The values in Table 3 were, of course, obtained with an independently set fast threshold.

Efficiency measurements by this technique can be made to better than one-half of one percent, but judging by our efforts carefully calculated efficiencies may be in error by as much as five percent at these energies. Another effort toward such measurements should include tests to determine the effects of multiple scattering of the helium particles in the target and the detector chamber and the effects of the C detector and the light piper. Additional effort would have to be made to resolve the calibration difficulties to ensure that calculational comparisons would be made for the

same minimum secondary particle energies. The technique provides a powerful and clean method for a routine calibration at neutron energies of 3 and 14 MeV. In addition to the efficiency measurements, timing checks may be made. For instance, time slewing observations as a function of pulse height can be made by observing the apparent neutron flight time corresponding to a series of narrow intervals in the pulse-height spectrum from the scintillator. Calibration of time-of-flight systems and pulse-shape discrimination tests can also be made.

ACKNOWLEDGMENTS

The authors wish to thank R. J. Schuttler of the University of Toulouse, France for his suggestions in the planning of these measurements and for his participation in the early phases of the experiment. They also thank V. V. Verbinski for his enlightening comments on the analysis of these data, as well as J. C. Courtney and W. R. Burrus for their assistance in adapting the 05R Monte Carlo code to this analysis. The efforts of H. A. Todd in the maintenance of the electronic equipment and those of O. W. Christian and H. Weaver in the operation of the accelerator are also appreciated. E. Beckham assisted greatly in the tedious work of data reduction.

REFERENCES

1. R. W. Peelle et al., Neutron Phys. Div. Ann. Progr. Rept. Aug. 1, 1963, ORNL-3499, Vol. II, pp. 73-79.

2. V. V. Verbinski, et al., Neutron Phys. Div. Ann. Progr. Rept. Aug. 1, 1963, ORNL-3499, Vol. I, pp. 108-115.

3. J. E. Hardy, Rev. Sci. Instr. 29, 8 (1958).

4. V. V. Verbinski, et al., Trans. Am. Nucl. Soc., 7 (2), 374 (1964).

5. K. F. Flynn et al., Nucl. Instr. Methods 27, 13 (1964).

6. L. Wichert, An Associated Particle Method for Measurements on Inelastic Scattering of D-D Neutrons, Thesis, Amsterdam University, Netherlands (1963).

7. F. G. J. Perey, Inelastic Scattering of 14-MeV Neutrons in Carbon Oxygen, and Lithium, Thesis, University of Montreal, Canada (1960).

8. A. Adam et al., Nucl. Instr. Methods 25, 365 (1964).

9. N. W. Hill and R. W. Peelle, Neutron Phys. Div. Ann. Progr. Rept. May 1, 1966, ORNL-3973, Sect. 9.4.

10. M. Forte, A. Kosta, and C. Maranza, pp. 277-286 in IAEA Proceedings of the Conference on Nuclear Electronics, Vol. II, 1962.

11. R. W. Peelle and T. A. Love, "Neutron Time-of-Flight Zero Cross Pulse Shape Discriminator," p. 196 in Proceedings of Conference Held at the U. S. Navy Postgraduate School, Nuclear Science Series Report No. 40, National Academy of Sciences (1964).

12. L. Blumberg and S. I. Schlesinger, Relativistic Tables of Energy and Angle Relationships for the $T(p,n)^3He$, $D(d,n)^3He$, and $T(d,n)^4He$ Reactions, AEC LJ-3118 (May 1956).

13. C. D. Zerby and H. S. Moran, Calculation of the Pulse Height Response of NaI(Tl) Scintillation Counters, ORNL-3169 (December 1961).

14. R. W. Peelle, Multiple Coulomb Scattering into a Detector in Charged Particle Coincidence Measurements Between Reaction Products, ORNL-TM-1517 (June 16, 1966).

15. R. T. Santoro et al., The Effects of Plastic Layers and Light Pipes on the Efficiency of Organic Scintillators for Neutron Detection, ORNL-3892 (to be published).

16. R. J. Shuttler, Efficiency of Organic Scintillators for Fast Neutrons, ORNL-3888 (1966).

17. N. A. Bostrom et al., Inelastic Scattering of Fast Neutrons From Nitrogen and Oxygen, WADC Technical Report 58-88 (February 1958).

18. D. D. Irving et al., O5R, A General Purpose Monte Carlo Neutron Transport Code, ORNL-3622 (February 1965).

19. M. Kalos and H. Goldstein, Neutron Cross Section Data for Carbon, NDA 12-16 (March 31, 1956).

20. V. V. Verbinski et al., The Response of Some Organic Scintillators to Fast Neutrons, Schielding Division Report ANS-SD-2 (December 1964).